

Unfolding collective AIS transmission behavior for vessel movement modeling on irregular timing data using noise-robust neural networks

Gabriel Spadon^a, Martha D. Ferreira^a, Amilcar Soares^b and Stan Matwin^{a,c,*}

^a*Institute for Big Data Analytics – Dalhousie University, 6299 South St, Halifax NS B3H 4R2, Canada*

^b*Department of Computer Science – Memorial University of Newfoundland, 230 Elizabeth Ave, St. John's NL A1C 5S7, Canada*

^c*Institute of Computer Science – Polish Academy of Sciences, Jana Kazimierza 5, Warsaw 525-000-94-01, Poland*

ARTICLE INFO

Keywords:

Automatic Identification System
Machine Intelligence
Ocean Science

ABSTRACT

This paper aims to model the Automatic Identification System (AIS) message transmission behavior through neural networks for forecasting the upcoming AIS messages' content for multiple vessels simultaneously in the face of messages' irregular timing. We present a set of experiments comprising tens of algorithms used for forecasting tasks with horizon sizes of varying lengths. Deep learning models revealed themselves to adequately capture the temporal irregularity while preserving the spatial awareness of different vessels. We show how a multi-directional and multi-layer long-short-term memory network and a convolution feature-extraction layer improve such a task by up to 20.01%.

1. Introduction

Over the years, we have been experiencing massive maritime vessel trajectory network¹ expansion powered by globalization and the evolution of transportation [1]. Maritime navigation has an essential role in passenger transportation, tourism, and fishing [2–7]. Besides, it has been historically used for trading between territories and countries worldwide [8–10]. Over the centuries, humankind has been forecasting the wind, waves, and weather to be prepared for non-ideal navigation conditions [11–13]. However, the ocean is far from controllable, and it bears dangers beyond nature, such as fires, piracy (e.g., armed robbery and hijackings), equipment defects, ship collisions, and others [14–20].

A convenient way of preventing or responding to these adverse events is observing vessels' trajectories through Automatic Identification System (AIS) messages [21], which are part of a more extensive system that monitors maritime navigation activity across space and time [22]. These messages are transmitted over radio or satellite at ideally periodic time intervals [23], containing information that identifies the vessel, the course and speed over the ground, and its geographical coordinates at message transmission [24]; that turns AIS into a plentiful source of spatiotemporal data and a supporting technology for monitoring vessel activities.

The literature on transportation systems has been leveraging AIS data's volume and sequential nature to develop various techniques for forecasting vessel trajectories [25–30]. The interest in accurate trajectory forecasting models comes from the capability to estimate vessel routes, which allows the analysis of situational awareness, assuring the integrity of the data transmitted by ships in the maritime vessel

trajectory network. In this context, the most popular techniques for trajectory forecasting are based on artificial neural networks, such as Recurrent Neural Networks (RNNs) [31–33], Auto-Encoder Neural Networks (AEs) [34–36], and Convolution Neural Networks (CNNs) [37]. These techniques satisfactorily forecast the trajectory of a few tens of vessels of the same type that navigate similar waters but pose a limitation when seeking generalization beyond that. Nevertheless, they provide insightful solutions to be translated into further maritime transportation challenges.

Despite vessels sending AIS messages periodically (e.g., every few seconds or minutes), the trajectories have irregular timing due to transmission delays, lack of signal coverage, and equipment defects. That irregular timing is a significant drawback to overcome by everyone working with AIS data because it can bring inconsistency in the vessel route, jeopardizing the maritime domain awareness [38]. Moreover, in some cases, such behavior might be deliberate and related to irregular maritime activities [39], but those are usually outliers among the population of messages.

In order to solve this issue, previous works in the literature have adopted a trajectory interpolation approach, which has been actively used as a resource for better trajectory planning and forecasting. Such an approach inserts virtual messages in the vessel trajectory to smooth the timing irregularity, allowing the trajectory to be strictly periodic [40, 41]. Therefore, the authors transform the AIS data into a well-behaved discrete-contained time series instead of proposing a solution in the face of raw and irregular series.

However, in the worldwide maritime vessel trajectory network, trajectory interpolation approaches can introduce uncertainty in vessel routes when the gap between two consecutive AIS messages is too large, which tends to alter the trajectory's data distribution. Such a disadvantage provides models that are not robust to irregular time, being driven to a subset of trajectories that cannot describe the maritime trajectories' network as a whole. Contrarily, adding the temporal component as a feature of the model and

*Corresponding author

✉ gabriel@spadon.com.br (G. Spadon); dais.martha@dal.ca (M.D. Ferreira); amilcarsj@mun.ca (A. Soares); stan@cs.dal.ca (S. Matwin)
ORCID(s): 0000-0001-8437-4349 (G. Spadon); 0000-0002-3078-9634 (M.D. Ferreira); 0000-0001-5957-3805 (A. Soares); 0000-0001-6629-8434 (S. Matwin)

¹Indistinctly referred in this work as a complex network, network, or graph.

accounting for irregular timing has the potential to provide models that better describe AIS messages continuously and simultaneously transmitted, improving generalization.

Along these lines, there is a lack of research exploring spatial and temporal features to improve the forecasting performance on irregular timing data. Accordingly, *we hypothesize that by leveraging spatial and temporal information from the AIS messages as features describing the inner states of the maritime vessel trajectory network rather than a single trajectory, it is possible to picture the future states of the network and provide a model capable of forecasting the content of future AIS messages for multiple vessels of different types indistinctly.* In such a scenario, machine intelligence and ocean science knowledge are joined to forecast the series that shape the vessel trajectory network for multiple vessels.

We believe that an efficient and robust way of modeling maritime vessel trajectory networks is based on including the irregular timing presented in the AIS data because it describes technical elements and challenges faced by the monitoring system. The addition of irregular timing in the models has the potential to improve safety in the sea, mainly in anticipating and responding accurately to emergencies in the transportation of goods and people, such as in the case of mechanical system failure or ship collision. In addition to real-time AIS messages, foreseen information can better picture the trajectories of multiple vessels of different types.

To the best of our knowledge, such an approach has not yet been studied from the perspective of maritime vessel trajectories due to its inherent timing complexity and volume of data in the form of AIS messages. Besides, it could set a milestone for future research along with similar premises. Therefore, to tackle this problem, we seek a model robust to different data distributions, irregular timing, and outliers.

In this context, we propose using an artificial neural network model composed of a multi-directional and multi-layer long-short-term memory network preceded by a convolution feature-extraction layer for achieving increased performance in predicting the intermediate states of the vessel trajectory network. Such a network was compared with tens of machine and deep learning models. Therefore, we also contributed with extensive experiments comparing different estimators and setting benchmarks for future research along similar lines. The results show that the proposed network improves the prediction of vessel routes when analyzing multiple vessels under different problem constraints. Besides, it was possible to observe the advantage of shallow deep-learning models over deeper ones for solving a challenging problem, which goes in the other direction from prior models.

Moreover, the results point out that traditional machine learning models struggle to generalize over different vessels, while deep learning models can better capture the temporal irregularity and spatial features while simultaneously describing multiple vessels' trajectories. In such a case, deep learning models achieve solid results over the competing algorithms, mainly when working with convolutional layers. In this context, we present a deep learning architecture

that achieve 2.37% improvement over highway transformer-based recurrent auto-encoder neural networks, 16.95% over transformer-based recurrent auto-encoder neural networks, 6.49% over traditional recurrent neural networks, 19.98% over recurrent highway networks, and 20.01% over feed-forward neural networks.

In conclusion, our contributions can be summarized as:

- A new perspective for AIS transmission behavior modeling accounting not only for the vessel trajectory but also for the full content of the AIS message under irregular timing constraints;
- A comprehensive benchmark with tens of machine and deep learning models submitted to the same forecasting task on horizon sizes of varying lengths;
- A methodological pipeline that describes how to capture the multiple data distributions on the temporal data for different vessel trajectories; and,
- A proposed model based on a multi-directional and multi-layer long-short-term memory network and a convolution feature-extraction layer to achieve increased performance on forecasting the AIS message content for multiple vessels regardless of vessel type.

In order to present our contributions, apart from the Introduction in Section 1, this article is organized into three sections. Section 2 states the problem, describes the dataset, and presents the methodology. Section 3 review the main results and discusses our findings. At last, Section 4 addresses the conclusions, future works, and final remarks. The supplementary material includes additional details of the algorithms used for experimentation and part of the experimental results not contained within the main article.

2. Methodology

2.1. Problem Formalization

AIS messages contain different types of information varying according to the monitoring necessities. In this paper, we defined an AIS message of a vessel as an event v , which is defined as $\vec{v} = \langle \rho, \gamma, \psi, \epsilon, \mu \rangle$, having latitude ρ , longitude γ , time ψ , COG (*i.e.*, Course Over Ground) ϵ and SOG (*i.e.*, Speed Over Ground) μ as attributes.

The sequence of AIS messages of a vessel composes its trajectory. Thus, we define the trajectory of a vessel as $\tau_i = \{V_{\tau_i}, E_{\tau_i}\}$, being a sequence of ordered events $v \in V_{\tau_i}$ connected by an edge $e \in E_{\tau_i}$. The edges are weighted by the distance \mathcal{D} between the source \vec{v}_n and target \vec{v}_{n+1} AIS messages, such that $e = \langle \vec{v}_n, \vec{v}_{n+1}, \mathcal{D}_{n,n+1} \rangle$, $\forall n \leq |V_{\tau_i}| - 1$.

A graph T can be built from these definitions considering all the vessel routes in the dataset. $T = \{\tau_0, \tau_1, \dots, \tau_c\}$ is a network of multiple connected components, in which $\tau_i \in T \forall 0 \leq i \leq c$ and c is the total number of different vessels. Knowing that different vessels cannot occupy the same space at the same time, T is under the condition that $V_{\tau_i} \cap V_{\tau_j} = \emptyset \wedge E_{\tau_i} \cap E_{\tau_j} = \emptyset, \forall \langle i, j \rangle \leq |T|, i \neq j$.

In terms of sequences and series, each trajectory $\tau \in T$ is composed of a sequence of ordered events $V_\tau = \langle \vec{v}_0, \vec{v}_1, \dots, \vec{v}_p \rangle$, where $p \in \mathbb{N}_+$ is the total number of events which varies for each vessel. The events are sets of spatiotemporal features describing the vessel trajectory information at different instants of time, such as given by $V_\tau = \langle \langle \rho, \gamma, \psi, \epsilon, \mu \rangle_0, \langle \rho, \gamma, \psi, \epsilon, \mu \rangle_1, \dots, \langle \rho, \gamma, \psi, \epsilon, \mu \rangle_p \rangle$.

In such a case, the problem for a single vessel can be defined as $f : x \subset V_\tau, x \in \mathbb{R}_+ \rightarrow \hat{y} \in \mathbb{R}$ and reduced to $f(x) \approx \hat{y}$, where f is the trajectory forecasting model that given a set x of observations will yield \hat{y} that resembles y the most, which refers to the future states of the trajectory. Accordingly, given an arbitrary optimization function $g : \mathbb{R}^2 \rightarrow \mathbb{R}_+$ computed between sets y and \hat{y} , in which $g(\hat{y}, y) \in \mathbb{R}_+$ and $\hat{y} \approx y$, we seek a model f that minimizes g for any $x \subset V_\tau$. Notice that x and y are contiguously contained in the series, but that does not mean that time between AIS messages is monotonically defined.

For purposes of network modeling, the problem of forecasting upcoming AIS messages based on historical AIS data for an arbitrary trajectory is unfeasible when using timestamps ψ as it follows a discrete probability distribution while other features are continuously defined. However, when including $\Delta T \in \mathbb{R}_+$, *i.e.*, the elapsed time since the last message, instead of timestamp ψ , the problem becomes feasible because the elapsed time also follows a continuous probability distribution. Thus, we have $V_\tau = \{ \langle \rho, \gamma, \Delta T, \epsilon, \mu \rangle_0, \dots, \langle \rho, \gamma, \Delta T, \epsilon, \mu \rangle_p \}$, $p \in \mathbb{N}_+$.

In such a scenario, the relationship between time events and delta time of a trajectory V_τ is given by $\psi_i - \psi_j = \Delta T_{ij}$, $\forall \langle i, j \rangle \leq |T|$, $i \neq j$ and $\psi_i + \Delta T_{ij} = \psi_j$, $\forall \langle i, j \rangle \leq |T|$, $i \neq j$, which means a timestamp can be safely inferred when one or a sequence of previous timestamps is known.

Motivated by the sequential nature of vessel trajectories, we aim to go further with the trajectory modeling problem by reconstructing the graph's topological structure and the features underneath its structure. That is possible because, in the case of vessel trajectories, the topology and features are deeply interconnected due to the spatiotemporal nature of the AIS messages. In such a scenario, the problem behaves non-scholastically, where the state of network node as \vec{v}^t depends on a sequence of $w \in \mathbb{N}_+$ past events $\vec{v}^t = \alpha_0 \vec{v}^{t-1} + \alpha_1 \vec{v}^{t-2} + \dots + \alpha_w \vec{v}^{t-w}$ subject to a set of scaling parameters $\vec{\alpha}$. We can define the previous relationship in terms of subsets $\bar{x} = \{ \langle \rho, \gamma, \Delta T, \epsilon, \mu \rangle_0, \dots, \langle \rho, \gamma, \Delta T, \epsilon, \mu \rangle_w \}$, $\bar{x} \subset \tau$ and $\bar{y} = \{ \langle \rho, \gamma, \Delta T, \epsilon, \mu \rangle_{w+1}, \dots, \langle \rho, \gamma, \Delta T, \epsilon, \mu \rangle_{w+s} \}$, $\bar{y} \subset \tau$, in which $w \in \mathbb{N}_+$ is the window of past observations and $s \in \mathbb{N}_+$ is the horizon to be predicted, subject to $w + s \leq |\tau|$.

Deeper in the analytical scenario, we now seek a function h that given \bar{x} will approximate \bar{y} , which can be written as $h : \mathbb{R}^{|\bar{x}|} \rightarrow \mathbb{R}^{|\bar{y}|}$. In such a case, h represents a function that better describes a trajectory network for any vessel or subset of vessels in the dataset, capable of picturing the inner states of the vessel trajectory network in the form of AIS messages.



Figure 1: A cylindrical-projected map depicting the region that comprises every trajectory in the dataset of AIS messages. Such a region is a bounding-box from coordinates 23°52'14.8"N 82°46'58.2"W and 68°30'02.8"N 2°01'18.4"W. The concerned trajectories were collected between March 2020 and July 2020.

2.2. Spatial Coverage

The dataset used along with this article comprises a portion of the Atlantic Ocean from Iceland to the south of the USA and the west of Europe to the north of Africa (see Figure 1). It consists of a private dataset provided by *exactEarth*² that contains raw AIS messages of over twenty thousand vessels of different types (*e.g.*, cargo, tanker, fishing, and other vessels) collected from March to July 2020, resulting in about sixty million AIS messages. It is worth noting that the vessels navigate independently, and they are not limited to navigating inside the bounding box that contains the dataset. Figure 2 was obtained when simultaneously visualizing all trajectories aided by an Edge Bundling visualization technique [42]. Although colors are used to contrast the flow of vessels, the thickness of the trajectories

² <https://www.exactearth.com/>

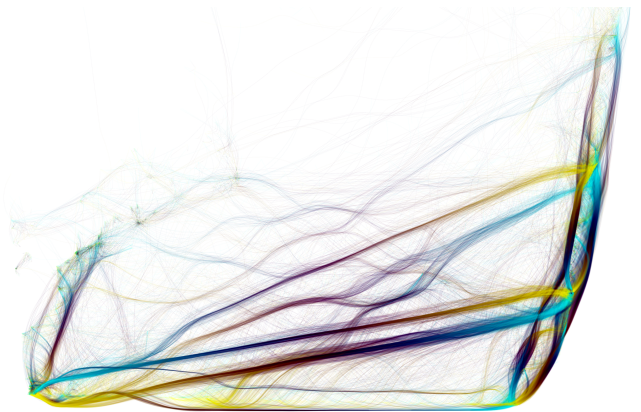


Figure 2: A kernel-based Edge Bundling visualization technique from Moura (2015) applied over the vessels trajectory network comprised in the bounding-box of coordinates 23°52'14.8"N 82°46'58.2"W and 68°30'02.8"N 2°01'18.4"W and using data collected between March and July 2020. The colors are arbitrarily used to contrast the flows and ease the visualization, while the thickness of the edges represents the flow intensity.

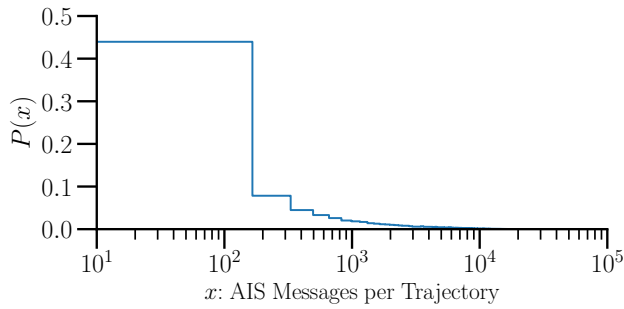


Figure 3: Probability distribution of Automatic Identification System (AIS) messages per trajectory (*i.e.*, vessel) in the dataset. The probability distribution shows that most vessels have few records, and a few vessels concentrate most of the records within the dataset. Accordingly, the distribution of AIS messages is comparable to a long-tail (*i.e.*, Pareto) distribution.

corresponds to the recurrent routes among the dataset, indicating the intensity of the maritime flow in that region.

These trajectories have different lengths as well as starting and ending locations. Next, Figure 3 illustrates the probability distribution of AIS messages per trajectory. Such a distribution has the shape of a long-tail (*i.e.*, Pareto) distribution, meaning that the dataset has most of its AIS messages concentrated on a small number of vessels trajectories and a few vessels dominate the trajectory dataset. Such an unbalanced dataset might come with a trade-off on performance and generalization for a forecasting task. In this case, different data modeling approaches must be considered to reduce the increased bias related to unbalanced datasets.

Besides that, the dataset has another conspicuous feature among the trajectories themselves, which is the irregular

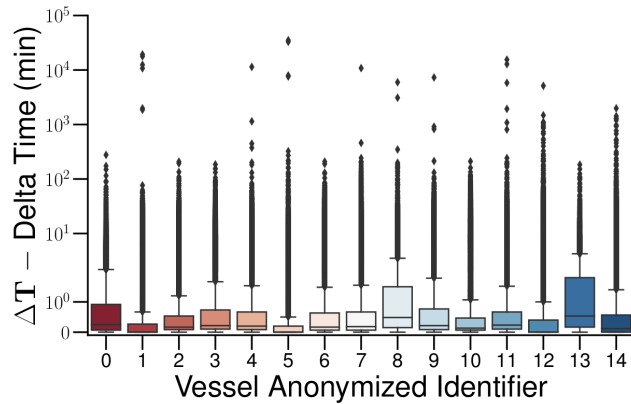


Figure 4: Interquartile range analysis of delta time divided by vessel identifier. For the analysis, we considered fifteen randomly selected vessels from the dataset ordered from the one with the most AIS messages on the left and the least on the right. The analysis reveals that, in terms of elapsed time distribution of AIS messages in a trajectory, all vessels present a severe presence of outliers. Such an outlier indicates the high irregularity of time between two AIS messages transmitted in an ordered vessel trajectory, varying from seconds to days.

timing phenomenon between consecutive transmitted AIS messages. For example, Figure 4 illustrates the phenomenon in the form of outliers observed between consecutive messages. The image provides the interquartile range analysis for fifteen randomly selected vessels, in which it is possible to note the extreme variance between consecutive transmissions in all different trajectories. Most messages are received within seconds or minutes, but there are recurrent cases where, due to transmissions delays, it reaches hours or days.

2.3. Window Sampling and Scaling

AIS data are notoriously known for their long historical sequences. Although its volume is considered an asset in many applications, its overabundance can also be detrimental, particularly in the face of unbalanced trajectories, as previously illustrated in Figure 3. To increase the model's vessel variability and geospatial range while it decreases the training time, we had to create a training technique based on temporal sampling. However, regular AIS message sampling affects the trajectory data distribution similarly to using trajectory interpolation based on virtual AIS messages (see Section 1), altering the behavior we seek to model.

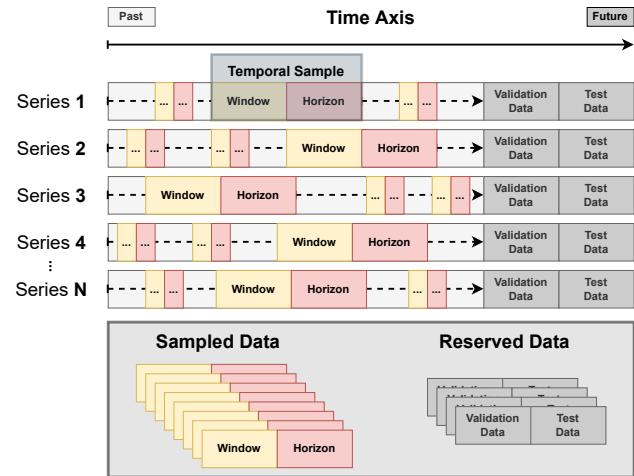


Figure 5: Temporal sampling technique used for increasing the variability of trajectories seen by the models. It decreases the computational time of training on the entire trajectories without increasing the timing irregularity within the windows. Through such an approach, the network sees segments of different vessel trajectories in varying timespans.

To preserve the data distribution, expand the model's capacity, and still reduce training time, we transformed each trajectory into predefined temporal segments known as windows, and then we sampled the temporal windows instead of the messages contained in them (see Figure 5). This approach preserves the course of time within the windowed AIS messages without increasing temporal irregularities inherent in message sampling. The idea is to sample sequences from all vessels indistinctly and feed them randomly to the learning model such that the model sees segments of trajectories from multiple vessels at varying timespans.

The data among the different sampled sequences are standardized using the z-score normalization, which enforces a zero mean and unit variance for all the records. Next, the standardized samples undergo a min-max normalization to set all values into a zero-one scale. All data transformation is applied on the variable axis shared among all the windowed samples of the dataset. The parameters for each transformation are computed from the training set samples only and then applied on the multiple samples of the testing data. Due to transforming the entire dataset, the output of all the modeling algorithms will follow a similar scale. Therefore, the output was inversely transformed to the original scale before assessing the results.

Along with the experiments, we have set a capstone of 25 windows for sampling from each trajectory in the dataset on all experiments. We refrain from sampling a higher number of windows because the higher the number of samples per different vessel trajectory, the longer the training sessions will be. Nevertheless, aiming at increasing the variability of sampling, the experiments are repeated five times using different random seeds, presenting as results the average of the experiments followed by their standard deviation. Such an approach allows us to work with a high number of vessels and preserves the irregular timing phenomenon, at the same time that it increases the reliability of the experimentation.

For training the model based on time-windowed data, the sliding window technique is a straightforward approach commonly used with sequence-and series-like data [43]. It works by setting a fixed-size window that slides over the temporal axis of the dataset, predicting a pre-specified number of future steps, referred to as horizon. Another possible approach is the expanding sliding window [44, 45]. Unlike the traditional technique, it starts with a preset window size that grows as it slides, iterating over longer sequences.

Due to the fact that neural network models are bound to the dimensions of the hidden weights of the model, all our experiments are based on the traditional sliding window technique. The dimensions of the hidden weights of the neural network are of a preset size and cannot be adjusted while training, as it would alter the number of internal parameters of the neural network on the fly, and neither traditional neural networks nor optimizers can handle it properly [46]. Moreover, the fixed window size is known for being a highly sensitive hyperparameter [47, 48], which leads us to set it before the experiments by considering the domain of the data and the dataset itself [46]. The window w and horizon s sizes used for experimentation along with the paper are presented as follows into three complexity categories:

1. Low Complexity: $w = 15$ & $s = 5$;
2. Medium Complexity: $w = 15$ & $s = 25$; and,
3. High Complexity: $w = 30$ & $s = 50$.

For the current dataset, most of the window sizes were set to be smaller than the horizon to increase the difficulty of the forecasting task, which will look to fewer past events for forecasting a larger horizon. However, forecasting sequences larger than the ones we used will increase the uncertainty

of the forecasting process and will stack the error of the sequentially forecasted AIS messages, possibly generating an output that no longer represents the target network. With that in mind, the different complexity cases were equally used in all experiments, and, along with the experiments in Section 3, we depict only the high complexity one. The other cases are contained in the supplementary material.

2.4. Optimization Strategy

The proposed neural network is trained using a mini-batch-based optimization strategy. In such a strategy, the algorithm iterates over the different samples of the dataset, feeding the network with mini-batches of different windowed data, repeating the process for all samples in random order. Feeding the neural network model with randomly ordered windowed data is imperative to achieve maximum generalization. Otherwise, the model could walk towards a *local optimum* due to recurrently focusing on samples of the same data distribution at the very beginning of the training process. In such a training fashion, the network parameters are shared among the dataset and optimized towards the *minima* of the loss function. We used AdamW [49] as the optimizer, a gradient descent-based algorithm. AdamW is a standard optimizer for sequence and series forecasting, being a variant of Adam [50] with weight regularization. In this scenario, the optimization criterion was the Hyperbolic Tangent Error (HTE), which is defined as follows:

$$\underset{\Omega}{\text{minimize}} \frac{1}{N} \sum_{i=1}^N (y_i - \hat{y}_i) \times \tanh(y_i - \hat{y}_i), \quad (1)$$

where Ω are the network parameters, N is the number of mini-batches, y is the ground-truth, and \hat{y} is the prediction.

The HTE behaves similarly to the traditional Mean Absolute Error (MAE), and both are less sensitive to outliers, but HTE allows for more refined results generalization in the face of the problem constraints observed in the trajectory network. The major difference between them is that the derivative, which is used to compute the gradients and update the network's weights, is a step function for the MAE and a non-linear function for the HTE. The optimization criterion is calculated from the full content of the AIS messages and not only the trajectory itself. In such a way, the overall error is a compound function of the individual errors of each variable in the message, which are all on the same scale (see Section 2.3). This way, the strategy is to find a model that minimizes all the variables within the messages.

2.5. Evaluation Metrics

In addition to the network optimization criterion, the results are presented with the aid of three other evaluation metrics, the Root Mean Squared Error (RMSE), Mean Absolute Error (MAE), and Huber Error (HE); defined as follows:

$$RMSE = \sqrt{\frac{1}{N} \sum_{i=1}^N (y_i - \hat{y}_i)^2} \quad (2)$$

$$MAE = \frac{1}{N} \sum_{i=1}^N |y_i - \hat{y}_i| \quad (3)$$

$$HE = \frac{1}{N} \sum_{i=1}^N L_i \quad (4)$$

$$\text{where } L_i = \begin{cases} 0.5 \times (y_i - \hat{y}_i)^2, & \text{if } |y_i - \hat{y}_i| < 1 \\ |y_i - \hat{y}_i| - 0.5, & \text{otherwise} \end{cases}$$

where y is the ground-truth, \hat{y} is the model prediction, and N is the number of mini-batches. The RMSE, based on the square root, is used to evaluate the model in the face of larger values, which in the case of the vessel trajectory network dataset are known to be outliers. Differently, the MAE can explain how the model handles the median values as it is less sensitive to outliers. Lastly, the HE is a smoothed version of the MAE that leverages the squared term when absolute error falls below one and the smoothed absolute error otherwise, providing another view of the median values while still being less sensitive to outliers. Identically to the optimization criterion, these performance evaluation metrics are computed from all the variables within the AIS message.

These metrics, including the Hyperbolic Tangent (HTE) used as loss function, are bound to $[0, \infty]$, where 0 indicates a perfect model under the light of that metric, and greater values indicate otherwise. It is noteworthy that, along with the results, predicting outliers is not the objective of the model; contrarily, a robust model will show satisfactory generalization among the median values regardless of the outliers. In other words, we seek a model that demonstrates a low average and standard deviation among HTE, HE, and MAE, but that does not necessarily reflect low RMSE values.

2.6. Network Architecture

The neural network we used for modeling the vessel trajectory network under irregular timing constraints and in the face of different data distributions is a bidirectional double-layered long-short-term memory (*i.e.*, LSTM [51]) network that operates with the aid of a one-dimensional convolution (*i.e.*, Conv1D [52]) feature-extraction layer. In such a case, after the windowing and window-sampling preparation processes (see Section 2.3), the data from the multiple trajectories is fed to a convolutional layer. In this layer, the multiple features existing within the windowed trajectories in a mini-batch (*i.e.*, input planes) will be combined into an intermediate tensor representation containing the hidden features that arise from the cross-correlation between the weights and the input planes. As a result of such a process, the hidden features will have the temporal axis dilated (or contracted) to match the number of output channels of the convolutional layer, initially set to be the window size w .

The one-dimensional convolution can be defined as:

$$x_t = \left(\sum_{p=0}^{\mathcal{I}-1} \mathbf{W}_{\mathcal{O}}^{(p)} \star x_N^{(p)} \right) + \mathbf{b}_{\mathcal{O}}, \quad (5)$$

where $\mathbf{W} \in \mathbb{R}^{\mathcal{O} \times \mathcal{I} \times k}$ is the weights, $\mathbf{b} \in \mathbb{R}^{\mathcal{O}}$ the bias, \star the cross-correlation operator, N the mini-batch size, k is the kernel size, \mathcal{O} the number of output channels, and \mathcal{I} the number of input channels — bounded to a sequence of size w , the sliding window's size. In this case, the output of the convolutional layer will be the hidden features with a temporal dimension matching the number of output channels.

Next, the hidden features extracted by the convolutional layer go through the first LSTM of the network, defined as:

$$\begin{aligned} i_t^{(1)} &= \sigma \left(\left(\mathbf{W}_{ii}^{(1)} \cdot x_t + \mathbf{b}_{ii}^{(1)} \right) + \left(\mathbf{W}_{hi}^{(1)} \cdot h_{t-1}^{(1)} + \mathbf{b}_{hi}^{(1)} \right) \right) \\ f_t^{(1)} &= \sigma \left(\left(\mathbf{W}_{if}^{(1)} \cdot x_t + \mathbf{b}_{if}^{(1)} \right) + \left(\mathbf{W}_{hf}^{(1)} \cdot h_{t-1}^{(1)} + \mathbf{b}_{hf}^{(1)} \right) \right) \\ g_t^{(1)} &= \tanh \left(\left(\mathbf{W}_{ig}^{(1)} \cdot x_t + \mathbf{b}_{ig}^{(1)} \right) + \left(\mathbf{W}_{hg}^{(1)} \cdot h_{t-1}^{(1)} + \mathbf{b}_{hg}^{(1)} \right) \right) \\ o_t^{(1)} &= \sigma \left(\left(\mathbf{W}_{io}^{(1)} \cdot x_t + \mathbf{b}_{io}^{(1)} \right) + \left(\mathbf{W}_{ho}^{(1)} \cdot h_{t-1}^{(1)} + \mathbf{b}_{ho}^{(1)} \right) \right) \\ c_t^{(1)} &= \left(f_t^{(1)} \circ c_{t-1}^{(1)} \right) + \left(i_t^{(1)} \circ g_t^{(1)} \right) \\ h_t^{(1)} &= o_t^{(1)} \circ \tanh \left(c_t^{(1)} \right), \end{aligned} \quad (6)$$

where $\mathbf{W}_i^{(1)}, \mathbf{W}_h^{(1)} \in \mathbb{R}^{\mathcal{O} \times \mathcal{O}}$ are the weights and $\mathbf{b}^{(1)} \in \mathbb{R}^{\mathcal{O}}$ the bias to be learned, $i_t^{(1)}$ is the input and update gate's activation vector, $f_t^{(1)}$ the forget gate's activation vector, $g_t^{(1)}$ the cell gate, $o_t^{(1)}$ the output gate's activation vector, $c_t^{(1)}$ the cell state vector, $h_t^{(1)}$ the hidden state vector, and σ the sigmoid activation function, \circ the Hadamard product.

The first LSTM cell will use the set of gates and memory for unfolding the sequences existing in the hidden features created from the cross-correlation operation. In such a way, it will incorporate traces of the multiple data distributions in the internal weights yielding an intermediate result that resembles the expected output. However, due to the increased complexity of working with outliers on multi-distribution data, an LSTM cell alone usually is not enough. In this case, we found that another memory cell could better picture the multiple behaviors existing in the trajectories and better represent the non-linearities inherent in the maritime vessel trajectory network. As a result, the hidden state vector of the first LSTM cell, *i.e.*, $h_t^{(1)}$, is then fed to a second LSTM cell creating a double-stacked LSTM formalized as follows:

$$\begin{aligned} i_t^{(2)} &= \sigma \left(\left(\mathbf{W}_{ii}^{(2)} \cdot h_t^{(1)} + \mathbf{b}_{ii}^{(2)} \right) + \left(\mathbf{W}_{hi}^{(2)} \cdot h_{t-1}^{(2)} + \mathbf{b}_{hi}^{(2)} \right) \right) \\ f_t^{(2)} &= \sigma \left(\left(\mathbf{W}_{if}^{(2)} \cdot h_t^{(1)} + \mathbf{b}_{if}^{(2)} \right) + \left(\mathbf{W}_{hf}^{(2)} \cdot h_{t-1}^{(2)} + \mathbf{b}_{hf}^{(2)} \right) \right) \\ g_t^{(2)} &= \tanh \left(\left(\mathbf{W}_{ig}^{(2)} \cdot h_t^{(1)} + \mathbf{b}_{ig}^{(2)} \right) + \left(\mathbf{W}_{hg}^{(2)} \cdot h_{t-1}^{(2)} + \mathbf{b}_{hg}^{(2)} \right) \right) \\ o_t^{(2)} &= \sigma \left(\left(\mathbf{W}_{io}^{(2)} \cdot h_t^{(1)} + \mathbf{b}_{io}^{(2)} \right) + \left(\mathbf{W}_{ho}^{(2)} \cdot h_{t-1}^{(2)} + \mathbf{b}_{ho}^{(2)} \right) \right) \\ c_t^{(2)} &= \left(f_t^{(2)} \circ c_{t-1}^{(2)} \right) + \left(i_t^{(2)} \circ g_t^{(2)} \right) \\ h_t^{(2)} &= o_t^{(2)} \circ \tanh \left(c_t^{(2)} \right), \end{aligned} \quad (7)$$

where $\mathbf{W}_i^{(2)} \in \mathbb{R}^{\mathcal{O} \times s}$ and $\mathbf{W}_h^{(2)} \in \mathbb{R}^{s \times s}$ are the weights and is $\mathbf{b}^{(2)} \in \mathbb{R}^s$ the bias; $i_t^{(2)}$ is the input/update, $f_t^{(2)}$ the

forget, and $o_t^{(2)}$ the output gate's activation vector; $g_t^{(2)}$ is the cell gate, $c_t^{(2)}$ the cell state vector, and $h_t^{(2)}$ the hidden state vector; σ the sigmoid activation function and \circ the element-wise Hadamard product. In such a case, the last hidden state of the second LSTM cell is the model's output. Due to the LSTM used being a bidirectional recurrent neural network, their hidden states are computed on the training process's forward and backward propagation phases, which will later be element-wise combined into \hat{y} and give shape to the inferred data of horizon s size, such as defined below:

$$\hat{y}_t = \overrightarrow{h_t^{(2)}} + \overleftarrow{h_t^{(2)}} \quad (8)$$

In another perspective, and depending on the size of kernel hyperparameter used for the single-dimensional convolution layer, the hidden features from the maritime vessel trajectory network tend to rise in dimension, creating a scrambled (*i.e.*, encoded) representation of trajectories similar to a latent space. It differs from a common latent space because, instead of a compressed representation in a lower dimension, the input tensor will have the features projected into a larger dimension, where the elements of the input planes tend to be better separated than they initially were. This sequential representation is then unfolded and translated into other sequences by the stacked LSTM cells, describing the trajectory network's future states in the face of different data distributions from the multiple trajectories.

Baselines

As a baseline, we considered over 60 different algorithms, comprising traditional and state-of-the-art ones. This experimental set includes machine and deep learning models adapted for the trajectory network modeling task, using the training preparation steps described in Sections 2.2 and 2.3.

The machine learning algorithms (see supplemental material for a complete list) come from open-source libraries, *e.g.*, scikit-learn [53], scikit-multiflow [54], scikit-extra³, lightning [55], and polylearn⁴. Other estimators, such as CatBoost [56], XGBoost [57], and LGBM [58], have their dedicated open-source implementation, which was preferred over others. It is noteworthy that most of these algorithms operate on a single-or multi-output sample space. However, even the more adaptable algorithm lacks straightforward support for both multi-output and multi-task forecasting problems, which are the case of having multiple vessels' trajectories describing time-varying variables.

Therefore, we adapt the single-output algorithms into multi-output ones using a *Regression Chain* mechanism⁵. This technique combines multiple single-output estimators of the same algorithm in the order specified by the chain, having one different estimator for each inferred horizon unit, in which the previous estimator feeds the following estimator [59]. However, even in a chained pipeline, these estimators cannot simultaneously focus on the multiple samples and variables. Therefore, the problem was split into

smaller parts, allowing the chained single-output and multi-output algorithms to focus on a single variable shared among all trajectories simultaneously, repeating the process for each variable in the dataset and then averaging the final results.

Through this approach, the inference process is simplified, as the algorithms are now centered on a single variable per time, instead of being required to forecast all of them simultaneously. However, it is important to note that, although the problem is more straightforward in terms of the number of variables simultaneously predicted, there is less interaction between multivariate samples, which might mean these estimators learn a limited amount of inter-variable features when compared to multi-output and multi-task ones.

In order to ease the understanding of the inference limitation of the baseline algorithms, along with the experiments, we have symbol-encoded them using the subsequent scale:

- ⊙ Represents single-output algorithms;
- ⊕ Indicates multi-output algorithms; and,
- Consists of multi-output and multi-task algorithms.

Specifically, among the deep learning baselines, we have used a different set of network architectures adapted and re-implemented for specifically handling the data from the vessel trajectory network. Related to Recurrent Neural Networks, we have conducted experiments with Elman's RNN [60], GRU [61], and LSTM [51]. For Auto-Encoders, we have used a simplification of ReGENN [46] for a bi-dimensional input, in which the Transformer Encoder [62] is used to extract an encoded representation from the input features, and an LSTM is used to decode such a representation into the horizon. Regarding Convolutional Neural Networks [63], we experimented on a temporal CNN with a single-dimension convolutional layer followed by a feed-forward layer that translates the output channels resulting from the cross-correlation operation into the horizon. Lastly, we experimented with a feed-forward network for accessing the results on a linear multi-output and multi-task estimator.

In addition, we have included an additional set of deep learning baselines, which are the highway networks [64, 65]. This is because time series estimators tend to lose the significance of the output predictions compared to the input when the information is propagated throughout the network repeatedly. Highway networks operate similarly to the auto-regression where the input is linearly re-scaled. Through a straight shortcut to the output, the re-scaled input is element-wise summed to the output from the other layers of the network to restore the scale of the data [66]. Such networks consist of a linear feed-forward layer that directly translates the input window w to the desired horizon s , such as follows:

$$\hat{y} = \mathbf{W} \cdot x + \mathbf{b} \equiv \left(\sum_{i=0}^w \mathbf{W}_{ih} \cdot x_{si} \right) + \mathbf{b}, \quad (9)$$

where $\mathbf{W} \in \mathbb{R}^{w \times s}$ are the weights and $\mathbf{b} \in \mathbb{R}^s$ the bias to be learned. The input x of window size w is converted to the

³ Available at <https://bit.ly/3tqPg3f>.

⁴ Available at <https://bit.ly/3KfGVFw>.

⁵ Available at <https://bit.ly/3hBfxTA>.

partial output \bar{y} in which the temporal dimension is equal to the horizon s . In such a scenario, the general output of the neural network comes from the element-wise summation of $\hat{y} = \bar{y} + \tilde{y}$, where \bar{y} is the linear output of the highway linear layer and \tilde{y} is the output of the other neural network layers. Such a technique was experimented with the RNNs, Auto-Encoders, and our architecture that joins CNN and LSTM.

Hyperparameter Tuning

Along with the experimentation, we use the default hyperparameters for all algorithms. More specifically, for the machine-learning baselines, the hyperparameters come from the open-source library where they are included (see the supplementary material), and for the deep-learning ones, PyTorch's defaults. Among the deep learning baselines, we used a gradient norm-clipping of 1.0, a learning rate of $1e^{-3}$, zero-probability dropout, and a learning rate scheduler to reduce the learning rate by a quarter every three stalled epochs. For the CNNs, specifically, we have used a fixed kernel size of 3, padding the input with a stride of 1, so the output has the same shape as the input, but with an increased number of output channels when compared to the input channel, which matches the size of the pre-fixed window.

Nevertheless, as part of the results, we show how our network behaves when we change the number of output channels of the convolutional layer (between 8, 16, 32, 64, and 128 channels) and also when we vary the recurrent layer (between Elman's RNN, GRU, and LSTM) in addition to their number of stacked layers ranging between 1 and 3. All the experiments were repeated five times with different random seeds to increase the variability of the sampled data during the experimentation and the order that the networks will see each of the samples (see Section 2.3). The random seeds used were 2021, 2121, 2221, 2321, and 2421.

Computer Environment

The experiments related to machine-learning algorithms were conducted on a Linux-based system with 80 CPUs and 504 GB of RAM. The ones related to deep learning were carried out on another Linux-based system with 104 CPUs, 126 GB of RAM, and a GeForce RTX 3090 (Ampere).

Reproducibility

The dataset used in this paper is not available to the general public for download due to being a private dataset owned by *ExactEarth*. However, aiming at the reproducibility of the results, we provide the source code, the snapshot of the trained network, and a sample dataset on *GitHub*⁶, guiding the user on how the inference process should be carried out.

3. Results & Discussion

This section describes the results considering the most complex experimental setup as highlighted by Section 2.3. Due to the gradual transition in the problem complexity containing different window and horizon sizes, many tested

algorithms present divergent behavior. In this case, some of the algorithms could not answer all the experimental setups given their required computational resources and computing time. Thus, within the supplementary material, we present a comprehensive list of all the algorithms used and those that could not be computed in each of the experiments.

That said, Figure 6 presents the first results from the performance benchmarks on the prediction of the 50 subsequent AIS messages given the last 30 AIS messages observed. The image is intentionally divided into two pieces for better visualization as the algorithms cluster in two different scales. The results presented at the top of the image performed worse than those at the bottom. The clustered results contrast the different performance groups for the same task.

Machine learning algorithms are concentrated among the models at the top of Figure 6. As described in Section 2.6, these models rely on multiple estimators to infer the problem's multiple samples, instants of time, and variables. These models have a different number of estimators alternating between 5 to 250. In this case, 5 estimators refer to a different estimator trained per variable of the dataset, while for 250, we have an estimator per variable and another for each different horizon in the output sequence. Although many of these algorithms are successfully applied in different academic benchmarks and real-world industrial problems, it is possible to notice that increasing the number of estimators per model tends to worsen their performance.

More deeply in the analysis of the performance of the machine learning models, we have a *Control Model* among them that always yields the average of the input features and the output for all the horizons. Such a model divides the first set of estimators into two further pieces, as denoted by the colored dashed lines in Figure 6. This division means that estimators above the dashed line performed worse than the average, while those below performed better. A consistent horizon, which corresponds to the average input features, describes a vessel staled on a single location that has never moved during the horizon duration despite the other features among the AIS messages. In this case, performing worst than the average is a piece of evidence that these algorithms cannot represent the multiple nuances arising from various trajectories, mainly when those unfold through time.

On the other hand, models located below the dashed control line outperformed the average of the input features. Even so, their performance is inferior to other models based on a single estimator, such as deep learning models. In particular, *Huber* is the only model consisting of 250 different estimators located below the control line. This is related to the fact that it uses the Huber loss (see Section 2.5) to be more robust to outliers in the training process. The same can be observed with the *Linear SVR*, which is an ensemble of 5 estimators and has the MAE with the soft-margin criterion as its loss function, which helps it to be robust to outliers.

Other algorithms are based on linear regressors with different stochastic solvers or optimization mechanisms, such as *AdaGrad*, *SAG*, and *SAGA*. The reasonable performance of linear-based algorithms comes from the linear nature

⁶Available at <https://bit.ly/367kdj7>.

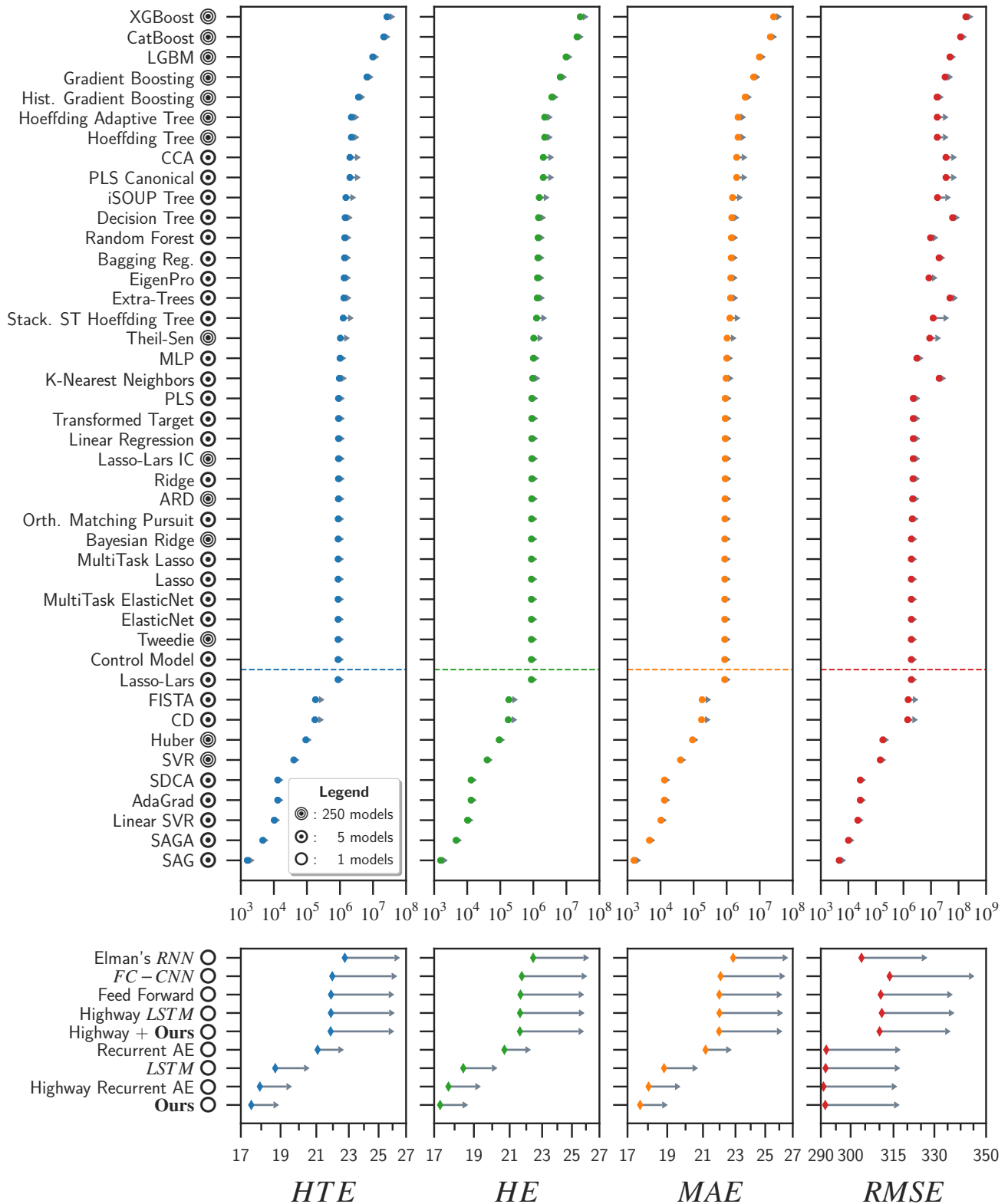


Figure 6: Performance estimation and comparison among different algorithms used for modeling the AIS transmission behavior. We have machine and deep learning algorithms clustered in two different segments according to their performance. The performance assessment is based on the Hyperbolic Tangent Error (HTE), Mean Absolute Error (MAE), Huber Error (HE), and the Root Mean Squared Error (RMSE). The experiments were conducted with algorithms on their out-of-the-box version with no hyperparameter optimization. Specifically, Elman's RNN, GRU, and LSTM are bidirectional. The estimators used the same dataset, but the deep learning baselines leveraged the HTE loss function and further training adaptation such as the ones used by our proposed model.

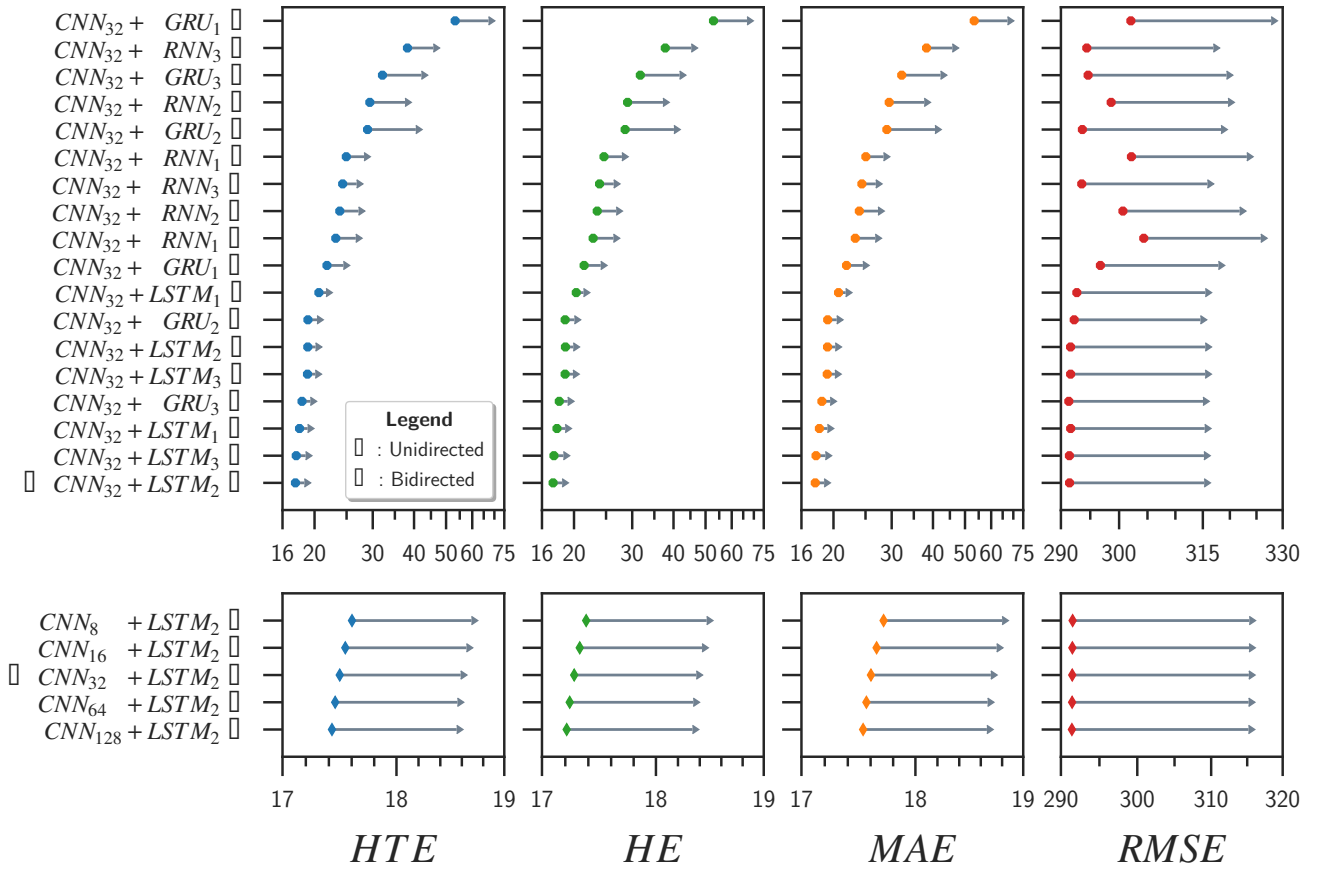


Figure 7: Impact analysis of different Recurrent Neural Networks (RNN) working in different directions and with a varying number of stacked layers compared to our proposed model for modeling the vessel trajectory network. In addition, the analysis of the impact of the output channels from the Convolutional Neural Network (CNN) in our proposed modeling approach. The performance assessment is based on the Hyperbolic Tangent Error (HTE), Mean Absolute Error (MAE), Huber Error (HE), and the Root Mean Squared Error (RMSE). Besides the ones indicated in the image, no other hyperparameter was changed.

of consecutive AIS messages, which do not incur many variations in the vessel coordinates besides their course and speed over the ground. A linear estimator can sufficiently model the problem for these particular cases. However, the problem becomes more complicated with the irregular temporal component of the AIS messages, which makes machine learning struggle over deep learning models.

The linear behavior of the trajectories can also be observed in more minor sequences when the time varies little and the presence of outliers tend to reduce. This refers to the low-complexity case of AIS messages prediction (see Section 2.3) included as part of the supplementary material. For such a specific scenario, we observed that highway networks and recurrent auto-encoders working together show better performance than our modeling approach on predicting the subsequent 5 AIS messages, such as pictured by Figure 1 in the Supplementary Material. In this case, our network is the second-placed among the algorithms. However, when the sequences start to increase, such as in the medium and high complexity cases, the behavior shifts in favor of our approach, showing that the hidden features extracted by the

convolutional layer and later processed through the long-short-term memory network can improve the solution.

For the high complexity case depicted in Figure 6, our model achieved 2.37% improvement over highway transformer-based recurrent auto-encoder neural networks, 16.95% over transformer-based recurrent auto-encoder neural networks, 6.49% over recurrent neural networks, 19.98% over recurrent highway networks, and 20.01% over feed-forward neural networks. For the medium complexity case, as depicted by Figure 3 in the Supplementary Material, it achieved 2.36% improvement over highway transformer-based recurrent auto-encoder neural networks, 13.50% over transformer-based recurrent auto-encoder neural networks, 14.08% over recurrent neural networks, 14.47% over recurrent highway networks, and 14.12% over feed-forward neural networks. For the low complexity case, as depicted by Figure 1 in the Supplementary Material, the highway transformer-based recurrent auto-encoder neural networks outperformed our model by 9.61%. As the second-placed, our model achieved 7.48% over transformer-based recurrent auto-encoder neural networks, 23.64% improvement over recurrent neural

networks, 19.05% over recurrent highway networks, and 17.61% over feed-forward neural networks.

Through this set of experiments, we observed that the behavior of neural networks diverges significantly according to the complexity of the sequence being predicted. So, for more minor sequences, models with fewer non-linearities tend to demonstrate better results than other more intricate models. This observation comes from the case of a feed-forward neural network being the third-placed for the case of lesser complexity (see Figure 1 in the Supplementary Material), showing better performance than any bidirectional recurrent neural network submitted to the same task. However, this behavior does not hold for all the models. For instance, the use of a highway neural network in parallel with our modeling approach jeopardizes performance in all complexity cases. The same is observed for highway recurrent neural networks.

3.1. Hyperparameters & Ablation

In Figure 7, we present the performance of the proposed model running on different hyperparameters. Specifically, the upper part of the image shows the impact of different recurrent neural networks operating in different directions and with varying numbers of layers. In the lower part of the image, the comparison is given by the increase in the number of output channels of the convolutional layer. Such results point out that bidirectional LSTMs show the best performance in solving the proposed problem and that the number of layers is related to the complexity of the problem, so more extensive sequences benefit from more stacked layers. However, the complexity of training multiple stacked LSTMs is greater than increasing the number of output channels of the convolution layer, which, in this case, presents itself as an alternative to reduce the network training time.

In fact, the adaptation of the output channels allows a better performance of the proposed model for the cases of medium and high complexity. This behavior can also be observed in Table 1, which presents the individual results of the neural network components in contrast with the optimized results from the adaptation of the number of output channels from the convolutional neural network. We observed that the double-stacked bidirectional LSTM shows suitable performance when alone in all three cases, but our modeling approach reaches further performance due to the application of the convolutional layer. The fully connected convolutional layer alone has not shown a favorable result compared to the others, but the highway transformer AE has behaved better than it in the medium and high complexity cases. Overall, the experiments showed favorably to the proposed modeling approach, which demonstrates to be the best-placed algorithm in two of the three tested cases under different horizon sizes.

3.2. Limitations

By including time as a feature of the model, we provide more information concerning the transmission behavior of AIS messages, which is essential for modeling transmissions. However, it also turns the problem into a more significant challenge for learning models due to the increased

Low Complexity	HTE	(+/-)
Highway Transformer AE	23.007	4.677
$CNN_{32} + LSTM_2^B$	25.455	4.668
$LSTM_2^B$	28.482	5.418
$FC - CNN$	28.011	6.214
Medium Complexity	HTE	(+/-)
Highway Transformer AE	19.466	1.205
$CNN_{128} + LSTM_2^B$	18.871	1.103
$LSTM_2^B$	19.068	1.141
$FC - CNN$	28.011	6.214
High Complexity	HTE	(+/-)
Highway Transformer AE	17.929	1.391
$CNN_{128} + LSTM_2^B$	17.427	1.125
$LSTM_2^B$	17.550	1.094
$FC - CNN$	21.962	3.974

Table 1

Detailed results for the proposed modeling approach and further network components describing the Hyperbolic Tangent Error (HTE) and the observed standard deviation.

uncertainty related to the irregular timing of messages. The irregular time observed between consecutive transmitted AIS messages is considered to be noise and it turns the AIS messages into outliers when the gap between two messages is too large. Such an issue would be reduced if working with smoothed trajectories because they include virtual AIS messages to fill the temporal gaps and interpolate the trajectory. However, that does not mean that the trajectories will be equally accurately pictured once interpolated due to not being free of uncertainty when the temporal gap is too large.

Besides that, it is evident that generalization and specification are opposite qualities of a learning model. That being said, our model behaves and generalizes better over multiple trajectories simultaneously. However, when a trajectory of a single vessel is of interest and when the historical AIS data from the vessel of interest is available, a model focused on that single data tends to yield better forecasting results over its trajectory. That is because models trained for forecasting the trajectory of a single vessel on the observed data of the vessel of interest will capture different behavior that is particular to that vessel. Regardless, on the task of predicting multiple trajectories simultaneously on the raw AIS data transmitted along with the vessel's trajectory, our modeling approach showed more robustness than other algorithms.

4. Conclusions

In this paper, we addressed the modeling of the AIS message transmission behavior through neural networks under noisy and temporally irregular data. We presented a comprehensive set of experiments comprising tens of machine and deep learning algorithms submitted to forecasting tasks with horizon sizes of varying lengths. Such a set of results show that traditional machine learning models strive to generalize over many vessels. Though, deep learning models revealed themselves to adequately capture the temporal irregularity while preserving the spatial awareness during forecasting the

trajectories of different vessels. In such a case, these models showed to be more robust to the AIS messages' irregular timing and delivered solid results over machine learning algorithms, mainly when combined with convolutional layers.

More specifically, joining long-short-term memory neural networks with single-dimension convolutional neural networks enhances the feature extraction process, increasing the neural network's performance under different circumstances. Our modeling approach was compared to multiple competing algorithms through an extensive set of experiments, where it showed a 2.36% and 2.37% improvement for medium and high complexity case scenarios over the Highway Recurrent Auto-Encoder Neural Network. Through such a multifaceted analysis of estimators' performance, we concluded that our modeling approach performs better on different sizes of sequences of AIS messages. Additionally, it allows further improvement by adapting the numbers of output channels of the convolution feature-extraction layer, which can either increase or decrease the number of temporal samples the multi-directional and multi-layer long-short-term memory network will use for training.

Nevertheless, much improvement can be achieved along with similar study premises. Those would be related to increasing the geographical boundary of AIS messages to a global scale, which would require greater computational power and processing time. Further improvement refers to using different modeling approaches for the AIS messages data, such as motif analysis on grid AIS data. Additionally, different neural network techniques, which require a different modeling approach not covered in this work, could enhance the interaction between trajectories. This is the case of Graph Neural Networks (GNNs), which might shape the relationship of the variables within the AIS messages.

Authors contributions statement

GS conceived the idea and planned the experiments. GS prepared the data for experimentation and conducted the experiments. MF analyzed the preliminary results. AS and SM reviewed the final results. GS wrote the original draft. MF, AS, and SM polished the main ideas and the paper. All authors reviewed and approved the results and manuscript.

Acknowledgments

The authors would like to thank *exactEarth* for the vessel trajectory network dataset used in this article and the Dalhousie Faculty of Computer Science for providing funding. The results are a contribution of the Canadian Foundation for Innovation MERIDIAN cyberinfrastructure⁷.

References

- [1] E. Carlini, V. M. de Lira, A. Soares, M. Etemad, B. Brandoli, S. Matwin, Understanding evolution of maritime networks from automatic identification system data, *GeoInformatica* (2021).

- [2] M. Luca, G. Barlacchi, B. Lepri, L. Pappalardo, A survey on deep learning for human mobility, *ACM Comput. Surv.* 55 (2021) 1–44.
- [3] L. M. Millefiori, P. Braca, D. Zisis, G. Spiliopoulos, S. Marano, P. K. Willett, S. Carniel, COVID-19 impact on global maritime mobility, *Scientific Reports* 11 (2021) 18039.
- [4] D. R. de Almeida, C. de Souza Baptista, F. G. de Andrade, A. Soares, A survey on big data for trajectory analytics, *ISPRS International Journal of Geo-Information* 9 (2020) 88.
- [5] P.-R. Lei, T.-H. Tsai, W.-C. Peng, Discovering maritime traffic route from AIS network, in: 2016 18th Asia-Pacific Network Operations and Management Symposium (APNOMS), IEEE, 2016, pp. 1–6.
- [6] S. Jennings, M. J. Kaiser, The effects of fishing on marine ecosystems, in: J. Blaxter, A. Southward, P. Tyler (Eds.), *Advances in Marine Biology*, volume 34 of *Advances in Marine Biology*, Elsevier, 1998, pp. 201–352.
- [7] T. R. Walker, O. Adebambo, M. C. D. A. Feijoo, E. Elhaimer, T. Hossain, S. J. Edwards, C. E. Morrison, J. Romo, N. Sharma, S. Taylor, S. Zomorodi, Environmental effects of marine transportation, in: C. Sheppard (Ed.), *World Seas: an Environmental Evaluation*, Elsevier, second edition edition, 2019, pp. 505–530.
- [8] C. Ducruet, The geography of maritime networks: A critical review, *Journal of Transport Geography* 88 (2020) 102824.
- [9] B. Wiegmans, P. Witte, M. Janic, T. de Jong, Big data of the past: Analysis of historical freight shipping corridor data in the period 1662–1855, *Research in Transportation Business & Management* 34 (2020) 100459. Data analytics for international transportation management.
- [10] M. T. Gastner, C. Ducruet, How heavy-tailed is the distribution of global cargo ship traffic?, in: 2014 Tenth International Conference on Signal-Image Technology and Internet-Based Systems, IEEE, 2014, pp. 289–294.
- [11] Y. Wang, R. Zou, F. Liu, L. Zhang, Q. Liu, A review of wind speed and wind power forecasting with deep neural networks, *Applied Energy* 304 (2021) 117766.
- [12] V. Kourafalou, P. D. Mey, M. L. Hénaff, G. Charria, C. Edwards, R. He, M. Herzfeld, A. Pascual, E. Stanev, J. Tintoré, N. Usui, A. van der Westhuysen, J. Wilkin, X. Zhu, Coastal ocean forecasting: system integration and evaluation, *Journal of Operational Oceanography* 8 (2015) s127–s146.
- [13] M. Papageorgiou, Coastal and marine tourism: A challenging factor in marine spatial planning, *Ocean & Coastal Management* 129 (2016) 44–48.
- [14] P. Chalk, Maritime piracy: Reasons, dangers and solutions, Technical Report, Rand Corp. Santa Monica – CA, 2009.
- [15] A. Bowden, The economic cost of maritime piracy, Technical Report, One Earth Future, 2010.
- [16] E. Marchione, S. D. Johnson, Spatial, temporal and spatio-temporal patterns of maritime piracy, *Journal of Research in Crime and Delinquency* 50 (2013) 504–524.
- [17] F. Goerlandt, P. Kujala, Traffic simulation based ship collision probability modeling, *Reliability Engineering & System Safety* 96 (2011) 91–107. Special Issue on Safecomp 2008.
- [18] M. Posada, H. Greidanus, M. Alvarez, M. Vespe, T. Cokacar, S. Falchetti, Maritime awareness for counter-piracy in the gulf of aden, in: 2011 IEEE International Geoscience and Remote Sensing Symposium, IEEE, 2011, pp. 249–252.
- [19] P. Chen, Y. Huang, J. Mou, P. van Gelder, Probabilistic risk analysis for ship-ship collision: State-of-the-art, *Safety Science* 117 (2019) 108–122.
- [20] L. M. Petry, A. Soares, V. Bogorny, B. Brandoli, S. Matwin, Challenges in vessel behavior and anomaly detection: From classical machine learning to deep learning, *Journal: Advances in Artificial Intelligence Lecture Notes in Computer Science* (2020) 401–407.
- [21] M. Robards, G. Silber, J. Adams, J. Arroyo, D. Lorenzini, K. Schwehr, J. Amos, Conservation science and policy applications of the marine vessel automatic identification system (AIS)—a review, *Bulletin of Marine Science* 92 (2016) 75–103.

⁷Learn more at <https://meridian.cs.dal.ca/>.

- [22] A. Soares, R. Dividino, F. Abreu, M. Brousseau, A. W. Isenor, S. Webb, S. Matwin, CRISIS: Integrating AIS and ocean data streams using semantic web standards for event detection, in: 2019 International Conference on Military Communications and Information Systems (ICMCIS), IEEE, 2019, pp. 1–7.
- [23] D. Yang, L. Wu, S. Wang, H. Jia, K. X. Li, How big data enriches maritime research – a critical review of automatic identification system (AIS) data applications, *Transport Reviews* 39 (2019) 755–773.
- [24] A. Harati-Mokhtari, A. Wall, P. Brooks, J. Wang, Automatic identification system (AIS): Data reliability and human error implications, *Journal of Navigation* 60 (2007) 373–389.
- [25] L. P. Perera, P. Oliveira, C. G. Soares, Maritime traffic monitoring based on vessel detection, tracking, state estimation, and trajectory prediction, *IEEE Transactions on Intelligent Transportation Systems* 13 (2012) 1188–1200.
- [26] G. Pallotta, M. Vespe, K. Bryan, Vessel pattern knowledge discovery from AIS data: A framework for anomaly detection and route prediction, *Entropy* 15 (2013) 2218–2245.
- [27] D. Nguyen, R. Vadaine, G. Hajduch, R. Garello, R. Fablet, A multi-task deep learning architecture for maritime surveillance using AIS data streams, in: 2018 IEEE 5th International Conference on Data Science and Advanced Analytics (DSAA), IEEE, 2018, pp. 331–340.
- [28] S. Patmanidis, I. Voulgaris, E. Sarri, G. Papavassilopoulos, G. Papavasileiou, Maritime surveillance, vessel route estimation and alerts using AIS data, in: 2016 24th Mediterranean Conference on Control and Automation (MED), IEEE, 2016, pp. 809–813.
- [29] Y. lun Zhang, P. fei Peng, J. shu Liu, S. kan Liu, AIS data oriented ships' trajectory mining and forecasting based on trajectory delimiter, in: 2018 10th International Conference on Intelligent Human-Machine Systems and Cybernetics (IHMSC), volume 01, IEEE, 2018, pp. 269–273.
- [30] M. Uney, L. M. Millefiori, P. Braca, Data driven vessel trajectory forecasting using stochastic generative models, in: ICASSP 2019 - 2019 IEEE International Conference on Acoustics, Speech and Signal Processing (ICASSP), IEEE, 2019, pp. 8459–8463.
- [31] C. Wang, H. Ren, H. Li, Vessel trajectory prediction based on AIS data and bidirectional GRU, in: 2020 International Conference on Computer Vision, Image and Deep Learning (CVIDL), IEEE, 2020, pp. 260–264.
- [32] J. Park, J. Jeong, Y. Park, Ship trajectory prediction based on bi-LSTM using spectral-clustered AIS data, *Journal of Marine Science and Engineering* 9 (2021) 1037.
- [33] P. Han, W. Wang, Q. Shi, J. Yang, Real-time short-term trajectory prediction based on GRU neural network, in: 2019 IEEE/AIAA 38th Digital Avionics Systems Conference (DASC), IEEE, 2019, pp. 1–8.
- [34] B. Murray, L. P. Perera, An AIS-based deep learning framework for regional ship behavior prediction, *Reliability Engineering & System Safety* 215 (2021) 107819.
- [35] B. Murray, L. P. Perera, A dual linear autoencoder approach for vessel trajectory prediction using historical AIS data, *Ocean Engineering* 209 (2020) 107478.
- [36] S. Capobianco, L. M. Millefiori, N. Forti, P. Braca, P. Willett, Deep learning methods for vessel trajectory prediction based on recurrent neural networks, *IEEE Transactions on Aerospace and Electronic Systems* 57 (2021) 4329–4346.
- [37] X. Chen, Y. Liu, K. Achuthan, X. Zhang, A ship movement classification based on automatic identification system (AIS) data using convolutional neural network, *Ocean Engineering* 218 (2020) 108182.
- [38] B. Tetreault, Use of the automatic identification system (AIS) for maritime domain awareness (MDA), in: Proceedings of OCEANS 2005 MTS/IEEE, IEEE, 2005, pp. 1590–1594 Vol. 2.
- [39] E. d'Afflisio, P. Braca, P. Willett, Malicious AIS spoofing and abnormal stealth deviations: A comprehensive statistical framework for maritime anomaly detection, *IEEE Transactions on Aerospace and Electronic Systems* 57 (2021) 2093–2108.
- [40] X. Li, Z. Feng, Y. Li, Z. Liu, R. W. Liu, Spatio-temporal vessel trajectory smoothing using empirical mode decomposition and wavelet transform, in: 2019 IEEE 4th International Conference on Big Data Analytics (ICBDA), IEEE, 2019, pp. 106–111.
- [41] X. Li, Z. Liu, Z. Liu, R. W. Liu, Z. Feng, Spatio-temporal vessel trajectory smoothing based on trajectory similarity and two-dimensional wavelet transform, in: 2019 5th International Conference on Transportation Information and Safety (ICTIS), IEEE, 2019, pp. 1500–1505.
- [42] D. C. Moura, 3D Density Histograms for Criteria-driven Edge Bundling, *ArXiv:1504.0268* (2015).
- [43] E. Keogh, S. Chu, D. Hart, M. Pazzani, Segmenting Time Series: a Survey and Novel Approach, in: *Series in Machine Perception and Artificial Intelligence*, volume Volume 57 of *Series in Machine Perception and Artificial Intelligence*, World Scientific, 2004, pp. 1–21.
- [44] E. Egrioglu, E. Bas, U. Yolcu, M. Y. Chen, Picture fuzzy time series: Defining, modeling and creating a new forecasting method, *Engineering Applications of Artificial Intelligence* 88 (2020) 103367.
- [45] A. Babii, R. T. Ball, E. Ghysels, J. Striaukas, Machine learning panel data regressions with an application to nowcasting price earnings ratios, *arXiv* (2020).
- [46] G. Spadon, S. Hong, B. Brandoli, S. Matwin, J. F. Rodrigues-Jr, J. Sun, Pay attention to evolution: Time series forecasting with deep graph-evolution learning, *IEEE Transactions on Pattern Analysis and Machine Intelligence* (2021) 1–1.
- [47] R. Frank, N. Davey, S. Hunt, Input window size and neural network predictors, in: Proceedings of the IEEE-INNS-ENNS International Joint Conference on Neural Networks. IJCNN 2000. Neural Computing: New Challenges and Perspectives for the New Millennium, volume 2, IEEE, 2000, pp. 237–242.
- [48] R. J. Frank, N. Davey, S. P. Hunt, Time series prediction and neural networks, *Journal of Intelligent and Robotic Systems: Theory and Applications* 31 (2001) 91–103.
- [49] I. Loshchilov, F. Hutter, Decoupled Weight Decay Regularization, *arXiv* (2017).
- [50] D. P. Kingma, J. Ba, Adam: A Method for Stochastic Optimization, in: Y. Bengio, Y. LeCun (Eds.), 3rd International Conference on Learning Representations, ICLR 2015 - Conference Track Proceedings, pp. 1–15.
- [51] S. Hochreiter, J. Schmidhuber, Long Short-Term Memory, *Neural Computation* 9 (1997) 1735–1780.
- [52] O. Abdeljaber, O. Avci, S. Kiranyaz, M. Gabbouj, D. J. Inman, Real-time vibration-based structural damage detection using one-dimensional convolutional neural networks, *Journal of Sound and Vibration* 388 (2017) 154–170.
- [53] F. Pedregosa, G. Varoquaux, A. Gramfort, V. Michel, B. Thirion, O. Grisel, M. Blondel, P. Prettenhofer, R. Weiss, V. Dubourg, J. Vanderplas, A. Passos, D. Cournapeau, M. Brucher, M. Perrot, E. Duchesnay, Scikit-learn: Machine learning in Python, *Journal of Machine Learning Research* 12 (2011) 2825–2830.
- [54] J. Montiel, J. Read, A. Bifet, T. Abdesslem, Scikit-multiflow: A multi-output streaming framework, *Journal of Machine Learning Research* 19 (2018) 1–5.
- [55] M. Blondel, F. Pedregosa, Lightning: large-scale linear classification, regression and ranking in Python, 2016.
- [56] L. O. Prokhorenkova, G. Gusev, A. Vorobev, A. V. Dorogush, A. Gulin, Catboost: unbiased boosting with categorical features, in: *NeurIPS*, pp. 6639–6649.
- [57] T. Chen, C. Guestrin, XGBoost: A scalable tree boosting system, in: Proceedings of the 22nd ACM SIGKDD International Conference on Knowledge Discovery and Data Mining, KDD '16, ACM, New York, NY, USA, 2016, pp. 785–794.
- [58] G. Ke, Q. Meng, T. Finley, T. Wang, W. Chen, W. Ma, Q. Ye, T.-Y. Liu, Lightgbm: A highly efficient gradient boosting decision tree, *Advances in neural information processing systems* 30 (2017) 3146–3154.

- [59] G. Melki, A. Cano, V. Kecman, S. Ventura, Multi-target support vector regression via correlation regressor chains, *Information Sciences* 415-416 (2017) 53–69.
- [60] J. Elman, Finding structure in time, *Cognitive Science* 14 (1990) 179–211.
- [61] J. Chung, C. Gulcehre, K. Cho, Y. Bengio, Empirical Evaluation of Gated Recurrent Neural Networks on Sequence Modeling, *arXiv* (2014).
- [62] A. Vaswani, N. Shazeer, N. Parmar, J. Uszkoreit, L. Jones, A. N. Gomez, Ł. Kaiser, I. Polosukhin, Attention is all you need, *Advances in Neural Information Processing Systems 2017-December* (2017) 5999–6009.
- [63] Y. Lecun, L. Bottou, Y. Bengio, P. Haffner, Gradient-based learning applied to document recognition, *Proceedings of the IEEE* 86 (1998) 2278–2324.
- [64] R. K. Srivastava, K. Greff, J. Schmidhuber, Highway Networks, *arXiv* (2015).
- [65] J. G. Zilly, R. K. Srivastava, J. Koutnik, J. Schmidhuber, Recurrent highway networks, *34th International Conference on Machine Learning, ICML 2017 8* (2017) 6346–6357.
- [66] G. Lai, W.-C. Chang, Y. Yang, H. Liu, Modeling Long- and Short-Term Temporal Patterns with Deep Neural Networks, in: *The 41st International ACM SIGIR Conference on Research & Development in Information Retrieval*, ACM, New York, NY, USA, 2018, pp. 95–104.

Supplementary Information

Unfolding collective AIS transmission behavior for vessel movement modeling on irregular timing data using noise-robust neural networks

Gabriel Spadon, Martha D. Ferreira, Amilcar S. Junior, Stan Matwin

List of Machine Learning Algorithms

#	Acronym	Name	Source
1	ARD	Automatic Relevance Determination Regression	https://bit.ly/3146kQA
2	AdaBoost	—	https://bit.ly/3qyfpd1
3	AdaGrad	—	https://bit.ly/3H1kITV
4	Adap. Random Forest	Adaptive Random Forest	https://bit.ly/32Fpywy
5	Bagging Reg.	Bagging Regressor	https://bit.ly/3Jo701f
6	Bayesian Ridge	—	https://bit.ly/3pxIINC
7	CCA	Canonical Correlation Analysis	https://bit.ly/3FE25K0
8	CD	Coordinate Descent	https://bit.ly/3Hj8UBG
9	CatBoost	—	https://bit.ly/3sFxET2
10	Decision Tree	—	https://bit.ly/33XoDbf
11	Control Model	Control Model	https://bit.ly/3FAB6EH
12	EigenPro	—	https://bit.ly/3pwh16M
13	ElasticNet	—	https://bit.ly/3mD43DD
14	Extra-Trees	—	https://bit.ly/3qzt97H
15	Factorization Machine	—	https://bit.ly/3qyxvvs
16	FISTA	FISTA	https://bit.ly/3puWRv3
17	Gamma	Generalized Linear Model with a Gamma distribution	https://bit.ly/32wofjI
18	Gaussian Process	Gaussian Process Regression	https://bit.ly/3zdvRUg
19	Gradient Boosting	—	https://bit.ly/3186FSs
20	Hist. Gradient Boosting	Histogram-based Gradient Boosting Regression Tree	https://bit.ly/3FuXt9D
21	Hoeffding Adaptive Tree	—	https://bit.ly/348avMF
22	Hoeffding Tree	—	https://bit.ly/3sFheaM
23	Huber	—	https://bit.ly/3sJpqqD
24	K-Nearest Neighbors	—	https://bit.ly/3186JSc
25	Kernel Ridge	—	https://bit.ly/3HmsD3F
26	LGBM	Light Gradient Boosting Machine	https://bit.ly/3HnTeNP
27	Lars	Least Angle Regression	https://bit.ly/3z5PywX
28	Lasso	—	https://bit.ly/32GkY0q
29	Lasso-Lars	—	https://bit.ly/3qyvFe2

#	Acronym	Name	Source
30	Lasso-Lars IC	Lasso-Lars with Information Criterion	https://bit.ly/3H1qLrA
31	Linear Regression	—	https://bit.ly/3FMuKgs
32	Linear SVR	Linear Support Vector Regression	https://bit.ly/3EEvnY5
33	MLP	Multi-layer Perceptron Regressor	https://bit.ly/3ewXJji
34	MultiTask ElasticNet	—	https://bit.ly/3H91h0i
35	MultiTask Lasso	—	https://bit.ly/3q098uf
36	NuSVR	Nu Support Vector Regression	https://bit.ly/3FCPQ0n
37	Orth. Matching Pursuit	Orthogonal Matching Pursuit	https://bit.ly/3JsaW18
38	PLS Canonical	Partial Least Square Canonical	https://bit.ly/3sJpUgr
39	PLS	Partial Least Squares	https://bit.ly/3JrNXGz
40	Passive Aggressive	—	https://bit.ly/3mFM9A1
41	Poisson	Generalized Linear Model with a Poisson distribution	https://bit.ly/3Hmyvdb
42	Polynomial Network	—	https://bit.ly/3pwjX4A
43	Quantile	—	https://bit.ly/3Jn6xQc
44	Radius Neighbors	—	https://bit.ly/32HYHj7
45	Random Forest	—	https://bit.ly/32tU78B
46	Ridge	—	https://bit.ly/3sDas08
47	SAGA	Stochastic Average Gradient Ascent	https://bit.ly/3mDzYDW
48	SAG	Stochastic Average Gradient	https://bit.ly/3quUt6R
49	SDCA	Stochastic Dual Coordinate Ascent	https://bit.ly/32tUa4h
50	SGD	Stochastic Gradient Descent	https://bit.ly/32zCvrP
51	SVR	Support Vector Regression	https://bit.ly/3pAK1dK
52	SVRG	Stochastic Variance Reduced Gradient	https://bit.ly/3HjBfI2
53	Stack. ST Hoeffding Tree	Stacked Single-target Hoeffding Tree	https://bit.ly/3qyIaGL
54	Theil-Sen	—	https://bit.ly/345f8ab
55	Transformed Target	—	https://bit.ly/3EvYFbr
56	Tweedie	—	https://bit.ly/3esTZb0
57	XGBoost	—	https://bit.ly/3z45dNr
58	iSOUP Tree	Incremental Structured Output Prediction Tree	https://bit.ly/3pHuFp7

Table 1: List of machine learning algorithms specifying their acronym, full name, and availability.

**Type of Algorithms
—— and ——
Usage on Experimentation**

#	Acronym	Type	15-05	15-25	30-50
1	ARD	⊙	✓	✓	✓
2	AdaBoost	⊙	✗	✗	✗
3	AdaGrad	⊙	✓	✓	✓
4	Adap. Random Forest	⊙	✗	✗	✗
5	Bagging Reg.	⊙	✓	✓	✓
6	Bayesian Ridge	⊙	✓	✓	✓
7	CCA	⊙	✓	✓	✓
8	CD	⊙	✓	✓	✓
9	CatBoost	⊙	✓	✓	✓
10	Decision Tree	⊙	✓	✓	✓
11	Control Model	⊙	✓	✓	✓
12	EigenPro	⊙	✓	✓	✓
13	ElasticNet	⊙	✓	✓	✓
14	Extra-Trees	⊙	✓	✓	✓
15	Factorization Machine	⊙	✓	✗	✗
16	FISTA	⊙	✓	✓	✓
17	Gamma	⊙	✗	✗	✗
18	Gaussian Process	⊙	✗	✗	✗
19	Gradient Boosting	⊙	✓	✓	✓
20	Hist. Gradient Boosting	⊙	✓	✓	✓
21	Hoeffding Adaptive Tree	⊙	✓	✓	✓
22	Hoeffding Tree	⊙	✓	✓	✓
23	Huber	⊙	✓	✓	✓
24	K-Nearest Neighbors	⊙	✓	✓	✓
25	Kernel Ridge	⊙	✗	✗	✗
26	LGBM	⊙	✓	✓	✓
27	Lars	⊙	✓	✓	✗
28	Lasso	⊙	✓	✓	✓
29	Lasso-Lars	⊙	✓	✓	✓
30	Lasso-Lars IC	⊙	✓	✓	✓
31	Linear Regression	⊙	✓	✓	✓
32	Linear SVR	⊙	✓	✓	✓
33	MLP	⊙	✓	✓	✓
34	MultiTask ElasticNet	⊙	✓	✓	✓
35	MultiTask Lasso	⊙	✓	✓	✓
36	NuSVR	⊙	✗	✗	✗
37	Orth. Matching Pursuit	⊙	✓	✓	✓
38	PLS Canonical	⊙	✓	✓	✓
39	PLS	⊙	✓	✓	✓
40	Passive Aggressive	⊙	✓	✓	✗
41	Poisson	⊙	✗	✗	✗
42	Polynomial Network	⊙	✓	✗	✗
43	Quantile	⊙	✗	✗	✗
44	Radius Neighbors	⊙	✗	✗	✗
45	Random Forest	⊙	✓	✓	✓

#	Acronym	Type	15-05	15-25	30-50
46	Ridge	⊙	✔	✔	✔
47	SAGA	⊙	✔	✔	✔
48	SAG	⊙	✔	✔	✔
49	SDCA	⊙	✔	✔	✔
50	SGD	⊙	✘	✘	✘
51	SVR	⊙	✔	✔	✔
52	SVRG	⊙	✘	✘	✘
53	Stack. ST Hoeffding Tree	⊙	✔	✔	✔
54	Theil-Sen	⊙	✔	✔	✔
55	Transformed Target	⊙	✔	✔	✔
56	Tweedie	⊙	✔	✔	✔
57	XGBoost	⊙	✔	✔	✔
58	iSOUP Tree	⊙	✔	✔	✔

Table 2: List specifying the type of each machine learning algorithm and the experiments where they were used. Along with the table, ⊙ to indicate multi-output algorithms, and ⊙ to refer to single-output algorithms. ✔ indicates whenever an algorithm was used with that specific experiment and ✘ indicates otherwise. An algorithm was removed from the pipeline whenever it could not provide results given the computational infrastructure available or when it took longer than seven days for training over the dataset for each experiment (*i.e.*, 15-05, 15-25, and 30-50).

Algorithms' Performance
—— for the ——
15-05 Experiment

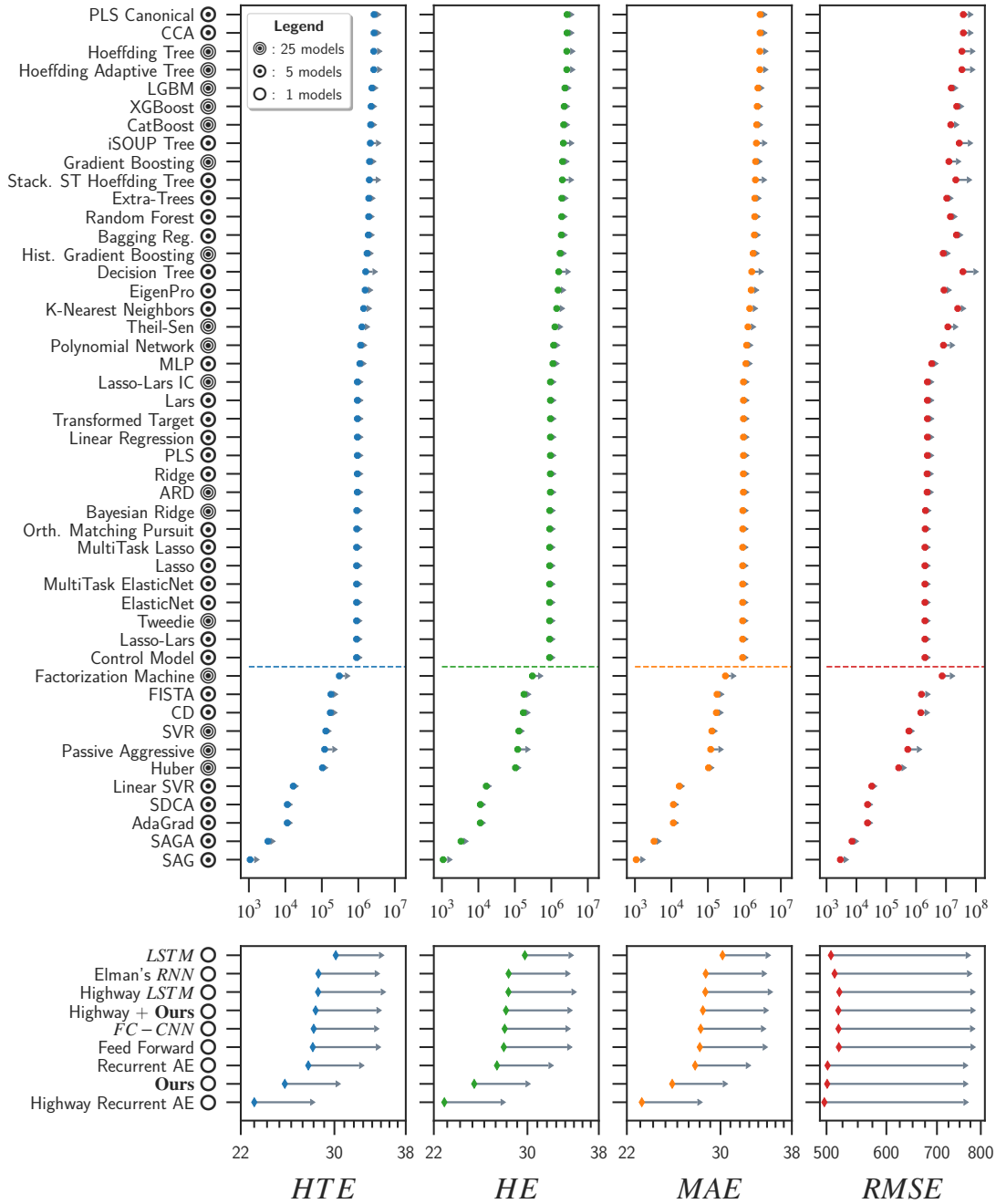


Figure 1: Performance estimation and comparison among different algorithms used for modeling the vessel trajectory network considering the low complexity case where algorithms look for the last 15 messages to predict the subsequent 5 messages. The performance assessment is based on the Hyperbolic Tangent Error (HTE), Mean Absolute Error (MAE), Huber Error (HE), and the Root Mean Squared Error (RMSE). The experiments were conducted with algorithms on their out-of-the-box version with no hyperparameter optimization. Specifically, Elman's RNN, GRU, and LSTM are bidirectional. The estimators used the same dataset, but the deep learning baselines leveraged the HTE loss function and further training adaptation used by our proposed model.

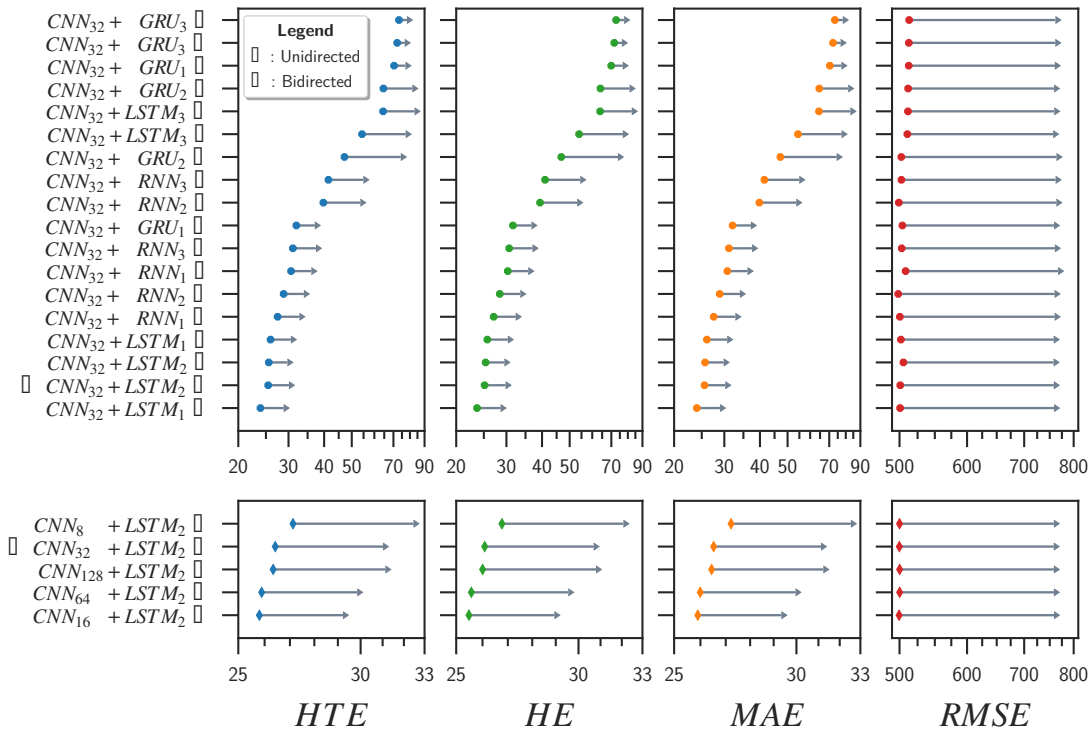


Figure 2: Impact analysis of different Recurrent Neural Networks (RNN) working in different directions and with a varying number of stacked layers compared to our proposed model for modeling the vessel trajectory network where algorithms look for the last 15 messages to predict the subsequent 5 messages. In addition to the analysis of the impact of the output channels from the Convolutional Neural Network (CNN) in our proposed modeling approach. The performance assessment is based on the Hyperbolic Tangent Error (HTE), Mean Absolute Error (MAE), Huber Error (HE), and the Root Mean Squared Error (RMSE). No further hyperparameter was changed.

Algorithms' Performance
—— for the ——
15-25 Experiment

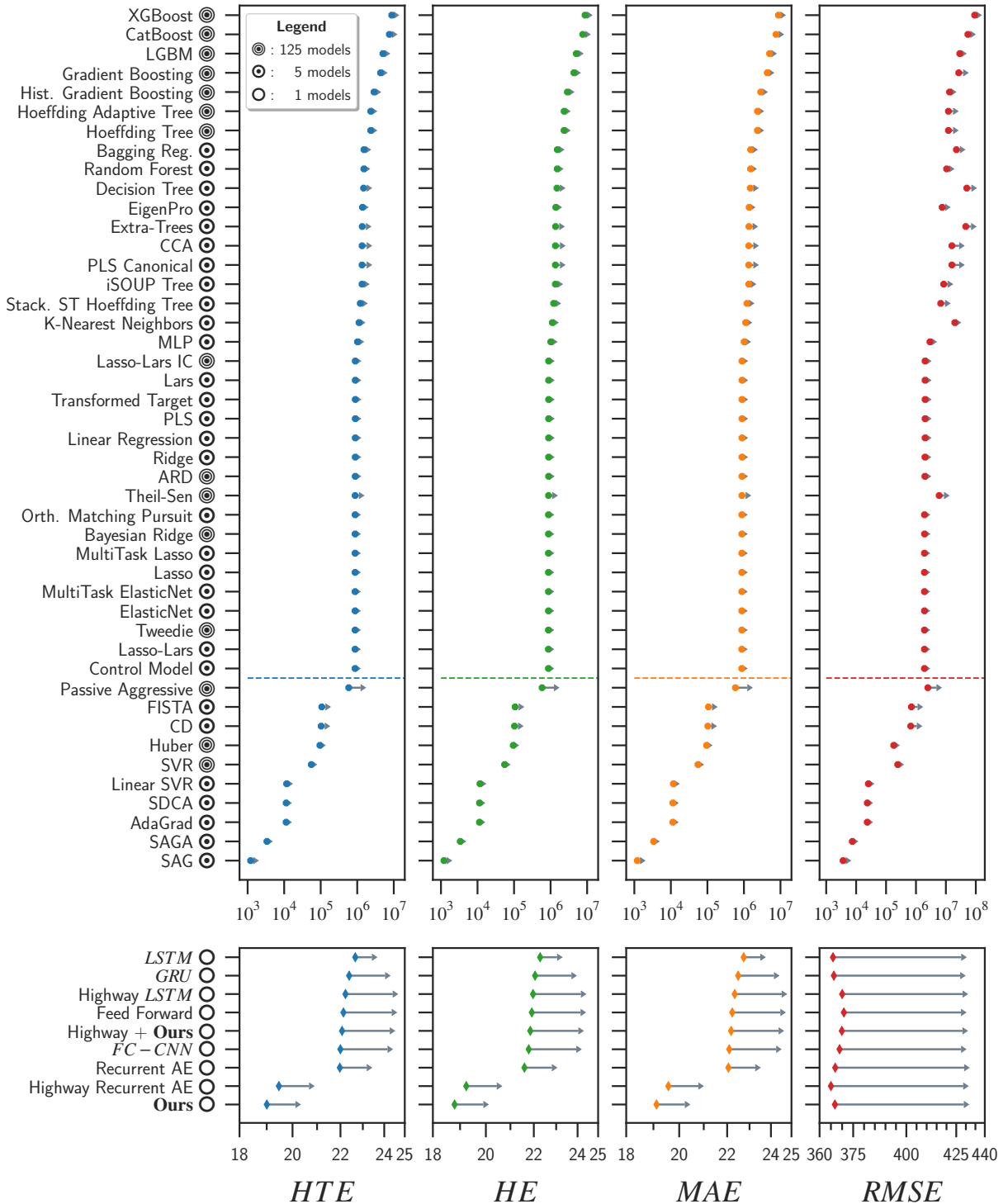


Figure 3: Performance estimation and comparison among different algorithms used for modeling the vessel trajectory network considering the low complexity case where algorithms look for the last 15 messages to predict the subsequent 25 messages. The performance assessment is based on the Hyperbolic Tangent Error (HTE), Mean Absolute Error (MAE), Huber Error (HE), and the Root Mean Squared Error (RMSE). The experiments were conducted with algorithms on their out-of-the-box version with no hyperparameter optimization. Specifically, Elman’s RNN, GRU, and LSTM are bidirectional. The estimators used the same dataset, but the deep learning baselines leveraged the HTE loss function and further training adaptation used by our proposed model.

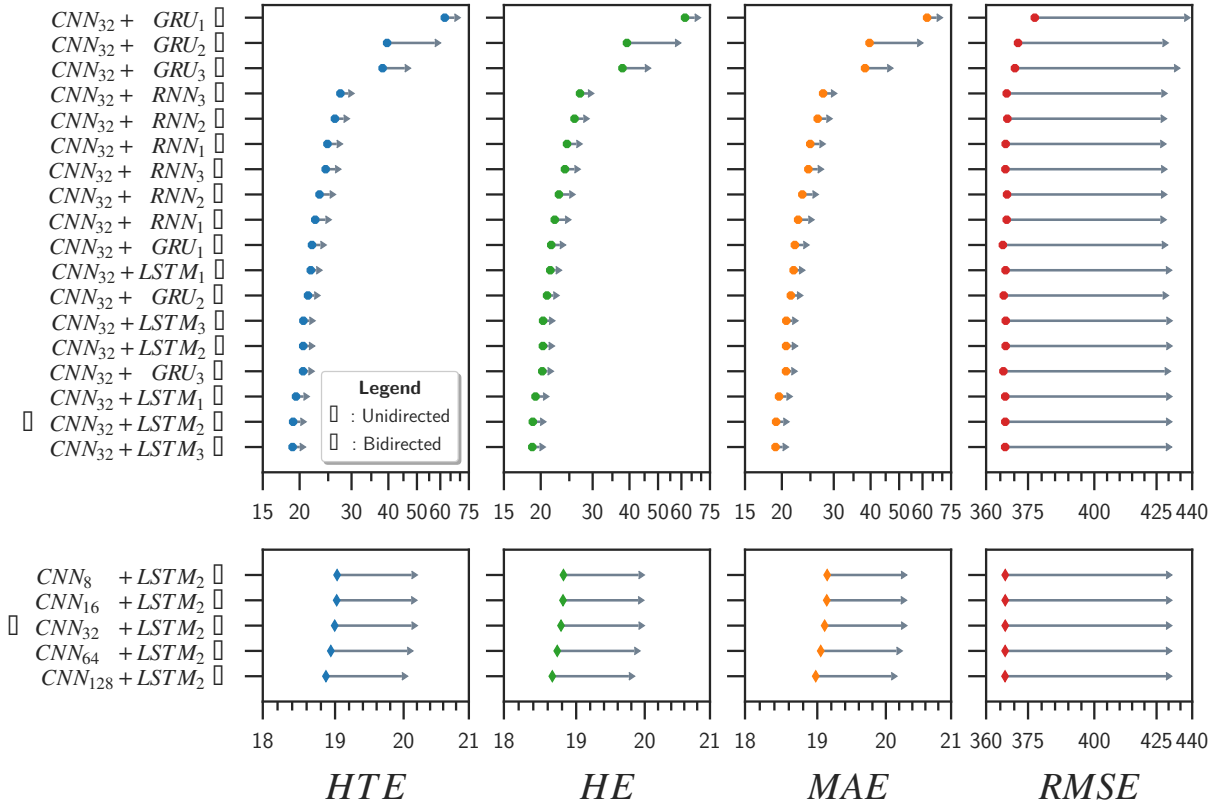


Figure 4: Impact analysis of different Recurrent Neural Networks (RNN) working in different directions and with a varying number of stacked layers compared to our proposed model for modeling the vessel trajectory network where algorithms look for the last 15 messages to predict the subsequent 25 messages. In addition to the analysis of the impact of the output channels from the Convolutional Neural Network (CNN) in our proposed modeling approach. The performance assessment is based on the Hyperbolic Tangent Error (HTE), Mean Absolute Error (MAE), Huber Error (HE), and the Root Mean Squared Error (RMSE). No further hyperparameter was changed.